

Search for the standard model Higgs boson in tau lepton pair final states

V.M. Abazov,³² B. Abbott,⁷⁰ B.S. Acharya,²⁶ M. Adams,⁴⁶ T. Adams,⁴⁴ G.D. Alexeev,³² G. Alkhazov,³⁶ A. Alton^{a,58} G. Alverson,⁵⁷ M. Aoki,⁴⁵ A. Askew,⁴⁴ S. Atkins,⁵⁵ K. Augsten,⁷ C. Avila,⁵ F. Badaud,¹⁰ L. Bagby,⁴⁵ B. Baldin,⁴⁵ D.V. Bandurin,⁴⁴ S. Banerjee,²⁶ E. Barberis,⁵⁷ P. Baringer,⁵³ J. Barreto,² J.F. Bartlett,⁴⁵ U. Bassler,¹⁵ V. Bazterra,⁴⁶ A. Bean,⁵³ M. Begalli,² L. Bellantoni,⁴⁵ S.B. Beri,²⁴ G. Bernardi,¹⁴ R. Bernhard,¹⁹ I. Bertram,³⁹ M. Besançon,¹⁵ R. Beuselinck,⁴⁰ V.A. Bezzubov,³⁵ P.C. Bhat,⁴⁵ S. Bhatia,⁶⁰ V. Bhatnagar,²⁴ G. Blazey,⁴⁷ S. Blessing,⁴⁴ K. Bloom,⁶¹ A. Boehnlein,⁴⁵ D. Boline,⁶⁷ E.E. Boos,³⁴ G. Borissov,³⁹ T. Bose,⁵⁶ A. Brandt,⁷³ O. Brandt,²⁰ R. Brock,⁵⁹ G. Brooijmans,⁶⁵ A. Bross,⁴⁵ D. Brown,¹⁴ J. Brown,¹⁴ X.B. Bu,⁴⁵ M. Buehler,⁴⁵ V. Buescher,²¹ V. Bunichev,³⁴ S. Burdin^{b,39} C.P. Buszello,³⁸ E. Camacho-Pérez,²⁹ B.C.K. Casey,⁴⁵ H. Castilla-Valdez,²⁹ S. Caughron,⁵⁹ S. Chakrabarti,⁶⁷ D. Chakraborty,⁴⁷ K.M. Chan,⁵¹ A. Chandra,⁷⁵ E. Chapon,¹⁵ G. Chen,⁵³ S. Chevalier-Théry,¹⁵ D.K. Cho,⁷² S.W. Cho,²⁸ S. Choi,²⁸ B. Choudhary,²⁵ S. Cihangir,⁴⁵ D. Claes,⁶¹ J. Clutter,⁵³ M. Cooke,⁴⁵ W.E. Cooper,⁴⁵ M. Corcoran,⁷⁵ F. Couderc,¹⁵ M.-C. Cousinou,¹² A. Croc,¹⁵ D. Cutts,⁷² A. Das,⁴² G. Davies,⁴⁰ S.J. de Jong,^{30,31} E. De La Cruz-Burelo,²⁹ F. Déliot,¹⁵ R. Demina,⁶⁶ D. Denisov,⁴⁵ S.P. Denisov,³⁵ S. Desai,⁴⁵ C. Deterre,¹⁵ K. DeVaughan,⁶¹ H.T. Diehl,⁴⁵ M. Diesburg,⁴⁵ P.F. Ding,⁴¹ A. Dominguez,⁶¹ A. Dubey,²⁵ L.V. Dudko,³⁴ D. Duggan,⁶² A. Duperrin,¹² S. Dutt,²⁴ A. Dyshkant,⁴⁷ M. Eads,⁶¹ D. Edmunds,⁵⁹ J. Ellison,⁴³ V.D. Elvira,⁴⁵ Y. Enari,¹⁴ H. Evans,⁴⁹ A. Evdokimov,⁶⁸ V.N. Evdokimov,³⁵ G. Facini,⁵⁷ L. Feng,⁴⁷ T. Ferbel,⁶⁶ F. Fiedler,²¹ F. Filthaut,^{30,31} W. Fisher,⁵⁹ H.E. Fisk,⁴⁵ M. Fortner,⁴⁷ H. Fox,³⁹ S. Fuess,⁴⁵ A. Garcia-Bellido,⁶⁶ J.A. García-González,²⁹ G.A. García-Guerra^{c,29} V. Gavrilov,³³ P. Gay,¹⁰ W. Geng,^{12,59} D. Gerbaudo,⁶³ C.E. Gerber,⁴⁶ Y. Gershtein,⁶² G. Ginther,^{45,66} G. Golovanov,³² A. Goussiou,⁷⁷ P.D. Grannis,⁶⁷ S. Greder,¹⁶ H. Greenlee,⁴⁵ G. Grenier,¹⁷ Ph. Gris,¹⁰ J.-F. Grivaz,¹³ A. Grohsjean^{d,15} S. Grünendahl,⁴⁵ M.W. Grünewald,²⁷ T. Guillemin,¹³ G. Gutierrez,⁴⁵ P. Gutierrez,⁷⁰ A. Haas^{e,65} S. Hagopian,⁴⁴ J. Haley,⁵⁷ L. Han,⁴ K. Harder,⁴¹ A. Harel,⁶⁶ J.M. Hauptman,⁵² J. Hays,⁴⁰ T. Head,⁴¹ T. Hebbeker,¹⁸ D. Hedin,⁴⁷ H. Hegab,⁷¹ A.P. Heinson,⁴³ U. Heintz,⁷² C. Hensel,²⁰ I. Heredia-De La Cruz,²⁹ K. Herner,⁵⁸ G. Hesketh^{f,41} M.D. Hildreth,⁵¹ R. Hirosky,⁷⁶ T. Hoang,⁴⁴ J.D. Hobbs,⁶⁷ B. Hoeneisen,⁹ M. Hohlfeld,²¹ I. Howley,⁷³ Z. Hubacek,^{7,15} V. Hynek,⁷ I. Iashvili,⁶⁴ Y. Ilchenko,⁷⁴ R. Illingworth,⁴⁵ A.S. Ito,⁴⁵ S. Jabeen,⁷² M. Jaffré,¹³ A. Jayasinghe,⁷⁰ R. Jesik,⁴⁰ K. Johns,⁴² E. Johnson,⁵⁹ M. Johnson,⁴⁵ A. Jonckheere,⁴⁵ P. Jonsson,⁴⁰ J. Joshi,⁴³ A.W. Jung,⁴⁵ A. Juste,³⁷ K. Kaadze,⁵⁴ E. Kajfasz,¹² D. Karmanov,³⁴ P.A. Kasper,⁴⁵ I. Katsanos,⁶¹ R. Kehoe,⁷⁴ S. Kermiche,¹² N. Khalatyan,⁴⁵ A. Khanov,⁷¹ A. Kharchilava,⁶⁴ Y.N. Kharzheev,³² I. Kiselevich,³³ J.M. Kohli,²⁴ A.V. Kozelov,³⁵ J. Kraus,⁶⁰ S. Kulikov,³⁵ A. Kumar,⁶⁴ A. Kupco,⁸ T. Kurča,¹⁷ V.A. Kuzmin,³⁴ S. Lammers,⁴⁹ G. Landsberg,⁷² P. Lebrun,¹⁷ H.S. Lee,²⁸ S.W. Lee,⁵² W.M. Lee,⁴⁵ J. Lellouch,¹⁴ H. Li,¹¹ L. Li,⁴³ Q.Z. Li,⁴⁵ J.K. Lim,²⁸ D. Lincoln,⁴⁵ J. Linnemann,⁵⁹ V.V. Lipaev,³⁵ R. Lipton,⁴⁵ H. Liu,⁷⁴ Y. Liu,⁴ A. Lobodenko,³⁶ M. Lokajicek,⁸ R. Lopes de Sa,⁶⁷ H.J. Lubatti,⁷⁷ R. Luna-Garcia^{g,29} A.L. Lyon,⁴⁵ A.K.A. Maciel,¹ R. Madar,¹⁵ R. Magaña-Villalba,²⁹ S. Malik,⁶¹ V.L. Malyshev,³² Y. Maravin,⁵⁴ J. Martínez-Ortega,²⁹ R. McCarthy,⁶⁷ C.L. McGivern,⁵³ M.M. Meijer,^{30,31} A. Melnitchouk,⁶⁰ D. Menezes,⁴⁷ P.G. Mercadante,³ M. Merkin,³⁴ A. Meyer,¹⁸ J. Meyer,²⁰ F. Miconi,¹⁶ N.K. Mondal,²⁶ M. Mulhearn,⁷⁶ E. Nagy,¹² M. Naimuddin,²⁵ M. Narain,⁷² R. Nayyar,⁴² H.A. Neal,⁵⁸ J.P. Negret,⁵ P. Neustroev,³⁶ T. Nunnemann,²² G. Obrant^{‡,36} J. Orduna,⁷⁵ N. Osman,¹² J. Osta,⁵¹ M. Padilla,⁴³ A. Pal,⁷³ N. Parashar,⁵⁰ V. Parihar,⁷² S.K. Park,²⁸ R. Partridge^{e,72} N. Parua,⁴⁹ A. Patwa,⁶⁸ B. Penning,⁴⁵ M. Perfilov,³⁴ Y. Peters,⁴¹ K. Petridis,⁴¹ G. Petrillo,⁶⁶ P. Pétroff,¹³ M.-A. Pleier,⁶⁸ P.L.M. Podesta-Lerma^{h,29} V.M. Podstavkov,⁴⁵ A.V. Popov,³⁵ M. Prewitt,⁷⁵ D. Price,⁴⁹ N. Prokopenko,³⁵ J. Qian,⁵⁸ A. Quadt,²⁰ B. Quinn,⁶⁰ M.S. Rangel,¹ K. Ranjan,²⁵ P.N. Ratoff,³⁹ I. Razumov,³⁵ P. Renkel,⁷⁴ I. Ripp-Baudot,¹⁶ F. Rizatdinova,⁷¹ M. Rominsky,⁴⁵ A. Ross,³⁹ C. Royon,¹⁵ P. Rubinov,⁴⁵ R. Ruchti,⁵¹ G. Sajot,¹¹ P. Salcido,⁴⁷ A. Sánchez-Hernández,²⁹ M.P. Sanders,²² B. Sanghi,⁴⁵ A.S. Santos^{i,1} G. Savage,⁴⁵ L. Sawyer,⁵⁵ T. Scanlon,⁴⁰ R.D. Schamberger,⁶⁷ Y. Scheglov,³⁶ H. Schellman,⁴⁸ S. Schlobohm,⁷⁷ C. Schwanenberger,⁴¹ R. Schwienhorst,⁵⁹ J. Sekaric,⁵³ H. Severini,⁷⁰ E. Shabalina,²⁰ V. Shary,¹⁵ S. Shaw,⁵⁹ A.A. Shchukin,³⁵ R.K. Shivpuri,²⁵ V. Simak,⁷ P. Skubic,⁷⁰ P. Slattery,⁶⁶ D. Smirnov,⁵¹ K.J. Smith,⁶⁴ G.R. Snow,⁶¹ J. Snow,⁶⁹ S. Snyder,⁶⁸ S. Söldner-Rembold,⁴¹ L. Sonnenschein,¹⁸ K. Soustruznik,⁶ J. Stark,¹¹ D.A. Stoyanova,³⁵ M. Strauss,⁷⁰ L. Stutte,⁴⁵ L. Suter,⁴¹ P. Svoisky,⁷⁰ M. Takahashi,⁴¹ M. Titov,¹⁵ V.V. Tokmenin,³² Y.-T. Tsai,⁶⁶ K. Tschann-Grimm,⁶⁷ D. Tsybychev,⁶⁷ B. Tuchming,¹⁵ C. Tully,⁶³ L. Uvarov,³⁶ S. Uvarov,³⁶ S. Uzunyan,⁴⁷ R. Van Kooten,⁴⁹ W.M. van Leeuwen,³⁰ N. Varelas,⁴⁶ E.W. Varnes,⁴² I.A. Vasilyev,³⁵ P. Verdier,¹⁷ A.Y. Verkheev,³² L.S. Vertogradov,³² M. Verzocchi,⁴⁵ M. Vesterinen,⁴¹ D. Vilanova,¹⁵ P. Vokac,⁷ H.D. Wahl,⁴⁴ M.H.L.S. Wang,⁴⁵ J. Warchol,⁵¹ G. Watts,⁷⁷ M. Wayne,⁵¹ J. Weichert,²¹ L. Welty-Rieger,⁴⁸

A. White,⁷³ D. Wicke,²³ M.R.J. Williams,³⁹ G.W. Wilson,⁵³ M. Wobisch,⁵⁵ D.R. Wood,⁵⁷ T.R. Wyatt,⁴¹ Y. Xie,⁴⁵ R. Yamada,⁴⁵ W.-C. Yang,⁴¹ T. Yasuda,⁴⁵ Y.A. Yatsunenko,³² W. Ye,⁶⁷ Z. Ye,⁴⁵ H. Yin,⁴⁵ K. Yip,⁶⁸ S.W. Youn,⁴⁵ J. Zennaro,⁶⁴ T. Zhao,⁷⁷ T.G. Zhao,⁴¹ B. Zhou,⁵⁸ J. Zhu,⁵⁸ M. Zielinski,⁶⁶ D. Zieminska,⁴⁹ and L. Zivkovic⁷²

(The D0 Collaboration*)

¹LAFEX, Centro Brasileiro de Pesquisas Físicas, Rio de Janeiro, Brazil

²Universidade do Estado do Rio de Janeiro, Rio de Janeiro, Brazil

³Universidade Federal do ABC, Santo André, Brazil

⁴University of Science and Technology of China, Hefei, People's Republic of China

⁵Universidad de los Andes, Bogotá, Colombia

⁶Charles University, Faculty of Mathematics and Physics,
Center for Particle Physics, Prague, Czech Republic

⁷Czech Technical University in Prague, Prague, Czech Republic

⁸Center for Particle Physics, Institute of Physics,
Academy of Sciences of the Czech Republic, Prague, Czech Republic

⁹Universidad San Francisco de Quito, Quito, Ecuador

¹⁰LPC, Université Blaise Pascal, CNRS/IN2P3, Clermont, France

¹¹LPSC, Université Joseph Fourier Grenoble 1, CNRS/IN2P3,

Institut National Polytechnique de Grenoble, Grenoble, France

¹²CPPM, Aix-Marseille Université, CNRS/IN2P3, Marseille, France

¹³LAL, Université Paris-Sud, CNRS/IN2P3, Orsay, France

¹⁴LPNHE, Universités Paris VI and VII, CNRS/IN2P3, Paris, France

¹⁵CEA, Irfu, SPP, Saclay, France

¹⁶IPHC, Université de Strasbourg, CNRS/IN2P3, Strasbourg, France

¹⁷IPNL, Université Lyon 1, CNRS/IN2P3, Villeurbanne, France and Université de Lyon, Lyon, France

¹⁸III. Physikalisches Institut A, RWTH Aachen University, Aachen, Germany

¹⁹Physikalisches Institut, Universität Freiburg, Freiburg, Germany

²⁰II. Physikalisches Institut, Georg-August-Universität Göttingen, Göttingen, Germany

²¹Institut für Physik, Universität Mainz, Mainz, Germany

²²Ludwig-Maximilians-Universität München, München, Germany

²³Fachbereich Physik, Bergische Universität Wuppertal, Wuppertal, Germany

²⁴Panjab University, Chandigarh, India

²⁵Delhi University, Delhi, India

²⁶Tata Institute of Fundamental Research, Mumbai, India

²⁷University College Dublin, Dublin, Ireland

²⁸Korea Detector Laboratory, Korea University, Seoul, Korea

²⁹CINVESTAV, Mexico City, Mexico

³⁰Nikhef, Science Park, Amsterdam, the Netherlands

³¹Radboud University Nijmegen, Nijmegen, the Netherlands

³²Joint Institute for Nuclear Research, Dubna, Russia

³³Institute for Theoretical and Experimental Physics, Moscow, Russia

³⁴Moscow State University, Moscow, Russia

³⁵Institute for High Energy Physics, Protvino, Russia

³⁶Petersburg Nuclear Physics Institute, St. Petersburg, Russia

³⁷Institució Catalana de Recerca i Estudis Avançats (ICREA) and Institut de Física d'Altes Energies (IFAE), Barcelona, Spain

³⁸Uppsala University, Uppsala, Sweden

³⁹Lancaster University, Lancaster LA1 4YB, United Kingdom

⁴⁰Imperial College London, London SW7 2AZ, United Kingdom

⁴¹The University of Manchester, Manchester M13 9PL, United Kingdom

⁴²University of Arizona, Tucson, Arizona 85721, USA

⁴³University of California Riverside, Riverside, California 92521, USA

⁴⁴Florida State University, Tallahassee, Florida 32306, USA

⁴⁵Fermi National Accelerator Laboratory, Batavia, Illinois 60510, USA

⁴⁶University of Illinois at Chicago, Chicago, Illinois 60607, USA

⁴⁷Northern Illinois University, DeKalb, Illinois 60115, USA

⁴⁸Northwestern University, Evanston, Illinois 60208, USA

⁴⁹Indiana University, Bloomington, Indiana 47405, USA

⁵⁰Purdue University Calumet, Hammond, Indiana 46323, USA

⁵¹University of Notre Dame, Notre Dame, Indiana 46556, USA

⁵²Iowa State University, Ames, Iowa 50011, USA

⁵³University of Kansas, Lawrence, Kansas 66045, USA

⁵⁴Kansas State University, Manhattan, Kansas 66506, USA

⁵⁵Louisiana Tech University, Ruston, Louisiana 71272, USA

⁵⁶Boston University, Boston, Massachusetts 02215, USA

- ⁵⁷Northeastern University, Boston, Massachusetts 02115, USA
⁵⁸University of Michigan, Ann Arbor, Michigan 48109, USA
⁵⁹Michigan State University, East Lansing, Michigan 48824, USA
⁶⁰University of Mississippi, University, Mississippi 38677, USA
⁶¹University of Nebraska, Lincoln, Nebraska 68588, USA
⁶²Rutgers University, Piscataway, New Jersey 08855, USA
⁶³Princeton University, Princeton, New Jersey 08544, USA
⁶⁴State University of New York, Buffalo, New York 14260, USA
⁶⁵Columbia University, New York, New York 10027, USA
⁶⁶University of Rochester, Rochester, New York 14627, USA
⁶⁷State University of New York, Stony Brook, New York 11794, USA
⁶⁸Brookhaven National Laboratory, Upton, New York 11973, USA
⁶⁹Langston University, Langston, Oklahoma 73050, USA
⁷⁰University of Oklahoma, Norman, Oklahoma 73019, USA
⁷¹Oklahoma State University, Stillwater, Oklahoma 74078, USA
⁷²Brown University, Providence, Rhode Island 02912, USA
⁷³University of Texas, Arlington, Texas 76019, USA
⁷⁴Southern Methodist University, Dallas, Texas 75275, USA
⁷⁵Rice University, Houston, Texas 77005, USA
⁷⁶University of Virginia, Charlottesville, Virginia 22901, USA
⁷⁷University of Washington, Seattle, Washington 98195, USA
(Dated: March 19, 2012)

We present a search for the standard model Higgs boson in final states with an electron or muon and a hadronically decaying tau lepton in association with zero, one, or two or more jets using data corresponding to an integrated luminosity of up to 7.3 fb^{-1} collected with the D0 detector at the Fermilab Tevatron collider. The analysis is sensitive to Higgs boson production via gluon gluon fusion, associated vector boson production, and vector boson fusion, and to Higgs boson decays to tau lepton pairs or W boson pairs. Observed (expected) limits are set on the ratio of 95% C.L. upper limits on the cross section times branching ratio, relative to those predicted by the Standard Model, of 14 (22) at a Higgs boson mass of 115 GeV and 7.7 (6.8) at 165 GeV.

PACS numbers: 13.85.Rm, 14.80.Bn

I. INTRODUCTION

The standard model (SM) of particle physics postulates a complex Higgs doublet field as the source of electroweak symmetry breaking, giving rise to non-zero masses of the vector bosons and fundamental fermions. The mass of the SM spin-zero Higgs boson, H , that survives after the symmetry breaking is not predicted, but is constrained by direct searches at the LEP [1], Tevatron [2] and LHC [3] colliders, to be in the range 115 – 127 GeV at the 95% C.L. Precision measurements of W and Z boson and top quark properties [4] indicate a SM Higgs boson mass, $m_H = 96^{+31}_{-24}$ [5]. Over the Higgs boson mass range $115 \leq m_H \leq 150$ the branching fractions vary considerably, with $H \rightarrow b\bar{b}$ ($H \rightarrow \tau^+\tau^-$) being the dominant (subdominant) decays for $m_H \leq 135$ GeV and $H \rightarrow W^+W^-$ ($H \rightarrow ZZ$) becoming important for $m_H > 135$ GeV. Previous analyses by the D0 and CDF

Collaborations have mainly focused on the decay modes $H \rightarrow b\bar{b}$ in the low mass region and $H \rightarrow WW$ with both W bosons decaying to an electron or muon in the high mass region.

A previous D0 publication [6] reported a Higgs boson search in the tau lepton pair plus two jets final state, with one tau decaying to a muon and the other to hadrons, using 1.0 fb^{-1} of data. In this Letter, we report the results of three searches involving tau pair production that extend the previous results by adding more data, increasing the trigger efficiency, adding new search channels, and considering additional signal contributions. The final states used are: (i) $\mu\tau$ plus zero or one jet (denoted $\mu\tau 0$), (ii) $\mu\tau$ plus two or more jets ($\mu\tau 2$), and (iii) $e\tau$ plus two or more jets ($e\tau 2$). The $\mu\tau 0$, $\mu\tau 2$, and $e\tau 2$ analyses use data collected with the D0 detector [7] corresponding to integrated luminosities of 7.3, 6.2 and 4.3 fb^{-1} respectively.

The Higgs boson production processes considered are (i) gluon gluon fusion (GGF), $gg \rightarrow H$ (+ jets); (ii) vector boson fusion (VBF), $q\bar{q} \rightarrow q\bar{q}H$; (iii) associated vector boson and Higgs boson production (VH), $q\bar{q} \rightarrow VH$, where V is a W or Z boson, and $V \rightarrow q\bar{q}$ (or $Z \rightarrow \nu\nu$ in the case of $\mu\tau 0$); and (iv) associated Higgs boson and Z boson production (HZ), $q\bar{q} \rightarrow HZ$, with $H \rightarrow b\bar{b}$ and $Z \rightarrow \tau\tau$. The GGF, VBF, and VH processes are further subdivided according to the Higgs boson decay, $H \rightarrow \tau\tau$,

*with visitors from ^aAugustana College, Sioux Falls, SD, USA, ^bThe University of Liverpool, Liverpool, UK, ^cUPIITA-IPN, Mexico City, Mexico, ^dDESY, Hamburg, Germany, ^eSLAC, Menlo Park, CA, USA, ^fUniversity College London, London, UK, ^gCentro de Investigacion en Computacion - IPN, Mexico City, Mexico, ^hECFM, Universidad Autonoma de Sinaloa, Culiacán, Mexico and ⁱUniversidade Estadual Paulista, São Paulo, Brazil. [‡]Deceased.

$H \rightarrow WW$, or (for the $\mu\tau 0$ analysis) $H \rightarrow ZZ$, and these subchannels are denoted as $\text{GGF}_{\tau\tau}$, GGF_{WW} or GGF_{ZZ} , etc. The fractional decompositions of signal contributions expected from Monte Carlo (MC) simulations are shown in Fig. 1 for the Higgs boson production cross section and branching ratios, and the event selection requirements, discussed below.

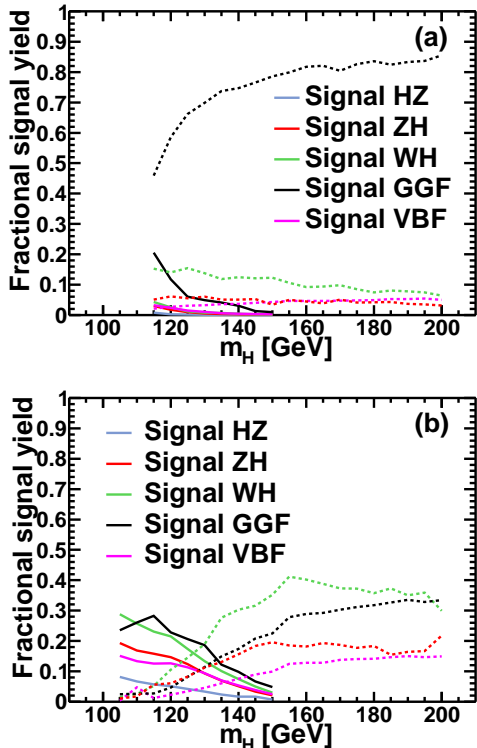


FIG. 1: (color online) Fractional yields for H signals from MC simulations as a function of M_H for (a) the $\mu\tau 0$ and (b) $\ell\tau 2$ analyses. The yields for each signal process are plotted as solid lines for $H \rightarrow \tau\tau$ decays and as dashed lines for the $H \rightarrow VV$ decays.

Tau leptons can occur either through direct decays of the Higgs boson (at low mass) or indirectly from $H \rightarrow VV$ with V decays to τs (at high mass). The leptons may arise from τ decay or (at high mass) directly from V decay. Thus the $\ell\tau$ channel is more uniformly sensitive to Higgs boson production over the full allowed mass range than are the dedicated $H \rightarrow b\bar{b}$ or $H \rightarrow WW \rightarrow \ell\ell\nu\nu$ analyses, thus improving the sensitivity of a combination of searches, particularly in the intermediate mass region around 135 GeV. In the following, “ τ ” represents a hadronically decaying tau and “lepton (ℓ)” denotes e or μ .

II. TRIGGER

The $\mu\tau 0$ and $\mu\tau 2$ data were collected using the full inclusive suite of triggers employed in D0. The trigger

efficiency for a subset of single muon triggers is measured to be about 65% using a sample of $Z \rightarrow \mu\mu$ events and is parameterized as a function of muon transverse momentum (p_T), pseudorapidity (η), azimuthal angle (ϕ), and instantaneous luminosity. Parametrizations of the efficiency functions are computed incorporating the observed luminosity distribution in the data and are applied to the MC simulations of the background and signal processes. The ratio of events from the inclusive trigger to those from the single muon triggers then establishes a multiplicative factor used to obtain the overall trigger efficiency. We examine the dependences of this ratio upon the p_T and η of the μ , τ and leading (highest p_T) jet. For the $\mu\tau 0$ analysis, the ratio is parameterized as a function of p_T^Z . For the lower statistics $\mu\tau 2$ analysis, no significant dependences are observed, and a constant scale factor is used. The use of the inclusive trigger gives an increase in the data sample of about 40% compared to that from the single muon triggers alone.

For the $e\tau 2$ analysis, a set of triggers requiring a single electromagnetic object was used. The efficiency of these triggers is obtained from an analysis of $Z \rightarrow ee$ events selected with just one identified electron and found to be about 85% efficient for the signal processes.

III. BACKGROUND AND SIGNAL SAMPLES

The major backgrounds for the Higgs boson search are Z + jets, W + jets, $t\bar{t}$, and multijet production (MJ) with misidentification of leptons or taus. Smaller backgrounds arise from boson (W, Z or γ) pair production and single top quark production. All but the MJ background are simulated using MC event generator programs and normalized to the highest available next-to-leading order (NLO) or next-to-NLO (NNLO) theoretical calculations. The MC simulations use the CTEQ6L1 parton distribution functions (PDF) [8].

The Z + jets and W + jets event samples are generated by ALPGEN [9], interfaced to PYTHIA [10] which provides initial and final state radiation and hadronization of the produced partons. The p_T^Z distribution is reweighted to agree with the D0 measurement [11]. The p_T^W is also reweighted for the $\ell\tau 2$ analyses using the reweighting factors derived for the p_T^Z distribution, multiplied by the ratio of the p_T^W to the p_T^Z distributions as predicted in NNLO QCD [12]. For the $\ell\tau 2$ analyses, the absolute normalization for the Z + jets and W + jets cross sections are taken from Ref. [13] using the MRST2004 NNLO PDFs [14]. The same Z + jets normalization is used for the $\mu\tau 0$ analysis but the W + jets normalization is derived from data as discussed below.

We simulate $t\bar{t}$ and single top quark events using the ALPGEN and COMPHEP [15] generators respectively, with PYTHIA used to simulate hadronization effects. The normalizations are based on the approximate NNLO calculations [16]. The diboson events are generated by PYTHIA.

Higgs boson production is simulated using PYTHIA,

with normalizations taken from Ref. [17]. We use HDECAY [18] and TAUOLA [19] to obtain the branching fractions of the Higgs boson and tau lepton respectively.

All MC signal and background events are input to a GEANT3-based [20] simulation of the detector response and processed with the same reconstruction programs as used for data. Data events collected from random beam crossings are superimposed on the MC events to account for detector noise and pileup from additional $p\bar{p}$ collisions in the same or previous bunch crossings. Correction factors are applied to the simulated events to account for the trigger efficiencies and for the differences between MC and data for the lepton, tau, and jet identifications, and for the energy scale and resolution of jets.

IV. EVENT SELECTION CRITERIA

Muons selected for this analysis are required to have hits in the muon chambers before and after the toroidal magnets and to be matched to a track in the tracking system with $p_T > 15$ GeV and $|\eta| < 1.6$. Muon candidates are required to be isolated in both the calorimeter and the tracking system using the calorimeter transverse energy, E_T^{iso} , in the annular cone $0.1 < \mathcal{R} < 0.4$ around the muon, where $\mathcal{R} = \sqrt{(\Delta\eta)^2 + (\Delta\phi)^2}$, and the track transverse momentum sum, $p_T^{\text{iso}} = \Sigma p_T^{\text{track}}$, within a cone $\mathcal{R} < 0.5$, excluding the p_T of candidate muon. For the $\mu\tau 0$ analysis, E_T^{iso} and p_T^{iso} must be less than 15% of p_T^μ . For the $\mu\tau 2$ analysis, E_T^{iso} and p_T^{iso} must be less than 2.5 GeV. Muon candidates due to cosmic rays are rejected if the scintillation counters surrounding the detector indicate a time of arrival more than 10 ns from that expected for collision products.

Electrons are identified using a likelihood variable, \mathcal{L}_e , that uses as inputs the quality of the matching of the electromagnetic (EM) shower centroid to a track, the fraction of energy deposited in the EM section of the calorimeter (EMF), a measure of the probability that the energy deposit pattern in the calorimeter conforms to that expected for an electron, E_T^{iso} , and the separation along the beam axis of the electron track and the primary vertex (PV) [21]. The signal sample electrons are required to have $\mathcal{L}_e > 0.85$. Electron candidate tracks are required to have $p_T > 15$ GeV and $|\eta| < 1.1$ or $1.5 < |\eta| < 2.5$, and to impinge upon a module of the central EM calorimeter within the central 80% of its azimuthal range.

The selection of hadronically decaying tau leptons is done separately for three types based on the number of tracks within a cone $\mathcal{R} < 0.3$ and the number of EM subclusters found in the calorimeter using a nearest neighbor algorithm. Type-1, patterned on the decay $\tau \rightarrow \pi\nu_\tau$, requires one track and no EM subclusters. Type-2, based on $\tau \rightarrow \rho(\pi^\pm\pi^0)\nu_\tau$, requires one track and at least one EM subcluster. Type-3, motivated by the $\tau \rightarrow \pi^\pm\pi^\pm\pi^\mp(\pi^0)\nu_\tau$ decay, requires at least two tracks with or without EM subclusters. We reject type-3 candidates with exactly two tracks of opposite signs since their

charge sign is ambiguous. The visible τ transverse energy, E_T^τ , is constructed from the tracking and calorimeter information. The track transverse momentum, p_T^{trk} , is the sum of the p_T of all tracks in the τ selection cone. We require $E_T^\tau > (12.5, 12.5, 15)$ GeV, $p_T^{\text{trk}} > (7, 5, 10)$ GeV, and $(p_T^{\text{trk}}/E_T^\tau) > (0.65, 0.5, 0.5)$ for τ types (1, 2, 3). The leading (highest p_T) track for type-3 τ s must exceed 7 GeV. A neural network, NN_τ [22], based on energy deposition patterns and isolation criteria in the calorimeter and tracking systems is constructed for each tau type to discriminate a tau from a misidentified jet. For type-2 τ leptons we discriminate taus from electrons using a second neural network, $\text{NN}_{\tau/e}$, constructed using variables that characterize the longitudinal and transverse energy profiles in the calorimeter, the energy and position correlations between τ tracks and calorimeter energy deposits, and isolation of the calorimeter energy.

Jets are selected using an iterative midpoint cone algorithm [23] with a cone size $\mathcal{R} = 0.5$. We require at least two tracks associated with the jet that point to the PV. Jet energies are corrected to the particle level for out-of-cone showering, underlying event energy deposits and pileup, and the estimated missing energy in jets with identified semileptonic decays of a hadron. Jets are corrected for energy scale and resolution; the MC jets are corrected for energy scale and resolution, as well as for the jet identification efficiency to bring the MC responses into agreement with data. For the quark-dominated MC samples ($t\bar{t}$ and diboson), there is an additional correction of the jet energy that accounts for the differences in the responses of quark jets and the dominantly gluon jets for which the jet energy scale correction was obtained. The $\mu\tau 2$ and $e\tau 2$ analyses require at least two jets with $|\eta_{\text{jet}}| < 3.4$ and $p_T^{\text{jet}} > 20$ (15) GeV for the leading (other) jet. The $\mu\tau 0$ analysis imposes these jet p_T requirements as a veto to ensure that the selected samples have no events in common.

The missing transverse energy, \cancel{E}_T , is computed from the observed transverse energy deposits in the calorimeter and is adjusted for the appropriate energy scale corrections for all objects and for isolated muons observed in the event. For the $\ell\tau 2$ analyses, the \cancel{E}_T is apportioned to the neutrinos from the two postulated tau leptons by decomposing the \cancel{E}_T vector into components associated with the observed lepton and hadronic tau [24].

For the final event selection, all three analyses require exactly one isolated lepton and a hadronic tau with opposite charges. The separations between all pairs of lepton, tau, and jet are required to be $\mathcal{R} > 0.5$. For the $\mu\tau 0$ analysis, events are required to have only one τ , and the smaller of the transverse masses, $m_T = \sqrt{2E_T^{\text{lepton}} \cancel{E}_T(1 - \cos\Delta\phi)}$ (where “lepton” = τ or μ and $\Delta\phi$ is the angle between the lepton and \cancel{E}_T) must exceed 25 GeV to suppress the Z + jets and MJ backgrounds, while retaining about 80% of the signal. For the $e\tau 2$ analysis, substantial backgrounds arise from Z + jets production with $Z \rightarrow ee$ where an electron is misidentified as

a type-2 τ . To reduce these, we remove τ candidates in the region $1.1 < |\eta| < 1.5$ where the calorimetry has impaired electron identification. Further Z + jets rejection is obtained by requiring type-2 τ candidates to have $NN_{\tau/e} > 0.95$ to suppress electrons that resemble the track + EM cluster signature. This cut retains more than 80% of type-2 τ s while rejecting about 90% of the electrons [25]. We reject type-2 τ candidates which point near the edge in ϕ of an EM module in the central calorimeter where the electron efficiency is low. In addition, type-3 τ candidates with $EMF > 0.95$ are excluded. The MJ background in the $e\tau 2$ analysis is suppressed by requiring $\mathcal{S} > 1$, where \mathcal{S} is a measure of the significance for \cancel{E}_T to differ from zero [26].

V. BACKGROUNDS DERIVED FROM DATA

The MJ background arising from misidentification of leptons or taus by the detector reconstruction algorithms is difficult to simulate, so for each analysis, the MJ background is taken from data. The general method for all analyses is similar: we define a sample of MJ-enriched events, \mathcal{M} , from which residual backgrounds simulated by MC are subtracted, to provide the shapes of the MJ kinematic distributions. The number of MJ events in the signal sample is obtained by multiplying the MJ yield in a signal-like sample \mathcal{N} by a scale factor ρ_i , obtained from the \mathcal{M} sample for each of the tau types, i . The ρ_i factors provide the estimate for the differences in the MJ background normalization between the \mathcal{N} and signal samples, based on the \mathcal{M} sample, and are in all cases within 10% of unity.

For the $\mu\tau 0$ channel, the sample \mathcal{M} is obtained by requiring $m_T(\mu, \cancel{E}_T) < 30$ GeV and $NN_\tau < 0.2$, and the ρ_i are the ratios of isolated to non-isolated lepton events in \mathcal{M} , and are parameterized as a function of $p_T^\tau, N_{\text{jets}}, \cancel{E}_T$, and p_T^μ . These factors scale the MJ fraction of the sample \mathcal{N} , selected as for the signal sample except that the muon is required to be non-isolated, to obtain the MJ normalization in the isolated lepton signal sample. An alternate MJ-enriched sample is defined by $NN_\tau < 0.2$ and $m_T(\mu, \cancel{E}_T) < 30$ GeV, in which the τ and μ have the same charge sign, for estimating the MJ background uncertainty.

For the $\mu\tau 2$ analysis, the MJ sample \mathcal{M} is obtained by reversing at least one of the muon isolation requirements and requiring $0.3 < NN_\tau < 0.8$. The MJ fraction of this sample is 94% before the MC-simulated background subtraction. The ρ_i factors are the ratio of opposite charge sign (OS) and same charge sign (SS) $\mu - \tau$ pairs in \mathcal{M} and are used to scale the MJ component of the sample \mathcal{N} selected as for the signal sample except that we require SS μ and τ . The ρ_i show no significant dependence on the kinematic variables.

For the $e\tau 2$ analysis, \mathcal{M} is obtained by requiring the electron to satisfy an orthogonal loose electron selection, $0 < \mathcal{L}_e < 0.85$, and $0.3 < NN_\tau < 0.9$. The MJ fraction of

this sample is 96% before the MC-simulated background subtraction. The ρ_i are obtained from the OS and SS \mathcal{M} sample and are applied to the MJ component of the \mathcal{N} sample as in the $\mu\tau 2$ analysis. The ρ_i show no significant dependence on kinematic variables. Alternate MJ-enriched samples, in which either the τ or lepton selections (but not both) are reversed, are defined for estimating the MJ background uncertainties in both $\ell\tau 2$ + analyses.

For the $\mu\tau 0$ analysis, the dominant background is from W + jets with the muon from W decay and a jet misidentified as a tau. Both the normalization of the W + jets sample and the misidentification probability are difficult to model adequately, so the simulation is corrected using a data-driven method [27]. The jet produced in association with a W boson has a charge that is correlated differently with the W boson charge for quarks and gluons. Furthermore, the probability for a jet misidentified as a tau to have the same charge sign as its progenitor parton varies with NN_τ . We determine a weight for W + jets MC events that depends on the charge correlation between the muon and recoil parton and on the value of NN_τ .

VI. EVENT YIELDS

The numbers of data and expected background events are given in Table I for the $\mu\tau 0$, $\mu\tau 2$, and $e\tau 2$ analyses.

TABLE I: For each analysis channel, the number of background events expected from MC simulated processes, MJ background, and observed data, for individual and sum of all tau types after preselection. “V+j” denotes W or Z + jets and “DB” denotes diboson processes.

τ type	$t\bar{t}$	$W+j$	$Z_{\ell\ell}+j$	$Z_{\tau\tau}+j$	DB	MJ	ΣBkd	Data
$\mu\tau 0$ analysis								
type 1	4	234	22	11	29	39	338	340
type 2	19	852	94	56	108	116	1245	1294
type 3	4	678	57	19	25	67	850	839
All	27	1764	172	86	162	223	2433	2473
$\mu\tau 2$ analysis								
type 1	13	9	5	29	2	19	76	81
type 2	86	57	22	159	12	59	394	418
type 3	13	34	4	43	3	22	119	109
All	112	100	31	231	16	99	589	608
$e\tau 2$ analysis								
type 1	2	2	0	6	1	6	18	10
type 2	14	21	14	30	2	25	106	98
type 3	7	16	2	11	1	15	52	59
All	24	40	16	46	4	47	176	167

VII. MULTIVARIATE ANALYSIS

The expected number of events for Higgs boson signal processes is small in comparison to the backgrounds

shown in Table I. For example, the expected signal yields at $m_H = 165$ GeV are 5.2, 1.7 and 0.3 events for the $\mu\tau 0$, $\mu\tau 2$ and $e\tau 2$ analyses respectively. The corresponding yields at $m_H = 115$ GeV are 0.9, 1.6 and 0.4 events. We thus employ multivariate techniques that utilize both the magnitudes of the variables and the correlations among them to separate the signal from the backgrounds. We choose well-modeled variables that have the capability to distinguish between at least one signal and one background as shown in Table II. Figure 2 shows distributions for representative variables that offer significant discrimination of signal and background for each of the channels.

TABLE II: List of variables used in the multivariate discriminants for the $\mu\tau 0$ and $\ell\tau 2$ analyses. The variable \cancel{E}_T is the missing transverse energy computed from the jets in the event.

Variable	$\mu\tau 0$	$\ell\tau 2+$
Lepton p_T	x	x
Tau p_T	x	x
Leading jet p_T	x	x
\cancel{E}_T	x	x
μ charge $\times \eta_\mu$	x	
η_τ	x	
$\ell\tau$ invariant mass	x	x
Dijet invariant mass		x
$\mu\tau$ \cancel{E}_T invariant mass	x	
$\ell\nu$ transverse mass, m_T^ℓ		x
$\tau\nu$ transverse mass, m_T^τ		x
Minimum of m_T^ℓ and m_T^τ	x	
$\Sigma \vec{p}_T $ of all jets		x
Scalar p_T sum of ℓ, τ, \cancel{E}_T , jets		x
Magnitude of vector p_T sum of ℓ, τ, \cancel{E}_T , jets		x
Minimum \sqrt{s} necessary for final objects	x	
Number of jets	x	
$\Delta\mathcal{R}$ between leading jets		x
$\Delta\eta$ between leading jets		x
Asymmetry between \cancel{E}_T and \cancel{E}_T		x
$\Delta\phi$ between ℓ and τ	x	
$\Delta\theta$ between ℓ and τ	x	
$\Delta\phi$ between ℓ and \cancel{E}_T	x	
$\Delta\phi$ between τ and \cancel{E}_T	x	
$\Delta\phi$ between \cancel{E}_T from calorimeter and tracks		x
Cosine of angle between ℓ and beam direction	x	
Minimum $\delta\phi$ between \cancel{E}_T and a jet		x
Missing E_T significance, \mathcal{S}		x
NN_τ	x	

The $\mu\tau 0$ analysis uses neural networks [28] (NN_H) trained to discriminate between all backgrounds and all signals for $115 \leq m_H \leq 200$ GeV in 5 GeV increments. Type-2 τ samples are trained separately, while the τ types 1 and 3 are combined for training to increase statistics. The NN_H distributions are binned in 21 equal sized bins for $0 < \text{NN}_H < 1.05$. The $\mu\tau 2$ and $e\tau 2$ analyses use boosted decision trees (BDT) [28] trained for all signals against the sum of all backgrounds, with all τ types combined for Higgs boson masses $105 \leq m_H \leq 200$ GeV in 5 GeV steps. The BDT output is binned in 15 bins spanning $-1 < \text{BDT} < 1$ with a non-uniform binning to assure sufficiently small statistical uncertainty in

the predicted backgrounds within any bin. We smooth the effects of signal MC statistics by averaging BDT distribution for m_H with the neighboring distributions at $(m_H - 5)$ GeV and $(m_H + 5)$ GeV with weights of 50%, 25%, and 25%. Figure 3 shows the NN_H distribution for the $\mu\tau 0$ analysis at $m_H = 165$ GeV and the averaged BDT distributions for the $\ell\tau 2$ analyses at $m_H = 150$ GeV.

VIII. SYSTEMATIC UNCERTAINTIES

A large number of systematic uncertainties have been considered, typically broken down separately for each analysis channel, tau type, background or signal process, or Higgs boson mass. The luminosity and trigger uncertainties are obtained from separate analyses of D0 data. The lepton, tau, and jet energy scale, resolution, and identification uncertainties are obtained from special control samples. Uncertainties in the MC-simulated background cross section normalizations and shapes are obtained using theoretical uncertainties, and the extent to which special data samples enriched in each background process agree with MC predictions. The MJ background uncertainties are determined by comparing the alternate MJ-enriched samples with the results obtained with the nominal choice. Signal cross section uncertainties are obtained from theoretical estimates and include the effect of PDF uncertainties. For each source, the impact on the final variable (NN_H or BDT) distribution is assessed by changing the nominal values of a parameter by ± 1 s.d. Some of the uncertainties affect only the normalization of the final variable distribution and some also modify its shape.

Table III summarizes the systematic uncertainties. Many entries comprise several subcategories. For example, the jet reconstruction uncertainty includes the effects of jet identification, confirmation that the tracks within the jet arise from the PV, jet resolution and jet energy scale. Moreover, these elements of the jet reconstruction uncertainty are computed separately for different background processes and hypothesized Higgs mass values in each analysis channel.

IX. CROSS SECTION LIMITS

We observe no excess of events over that expected from backgrounds in Fig. 3. We therefore obtain upper limits on the Higgs boson cross section for each analysis from the final multivariate outputs using the modified frequentist method [29], using a negative log likelihood ratio (LLR) for the background only and signal+background hypotheses as the test statistic. For the $\mu\tau 0$ analysis, each tau type is input separately to the limit setting calculation for Higgs boson masses from 115 to 200 GeV in 5 GeV steps. The $\ell\tau 2$ calculation uses the BDTs summed over tau type for m_H values from 105 to 200 GeV in 5

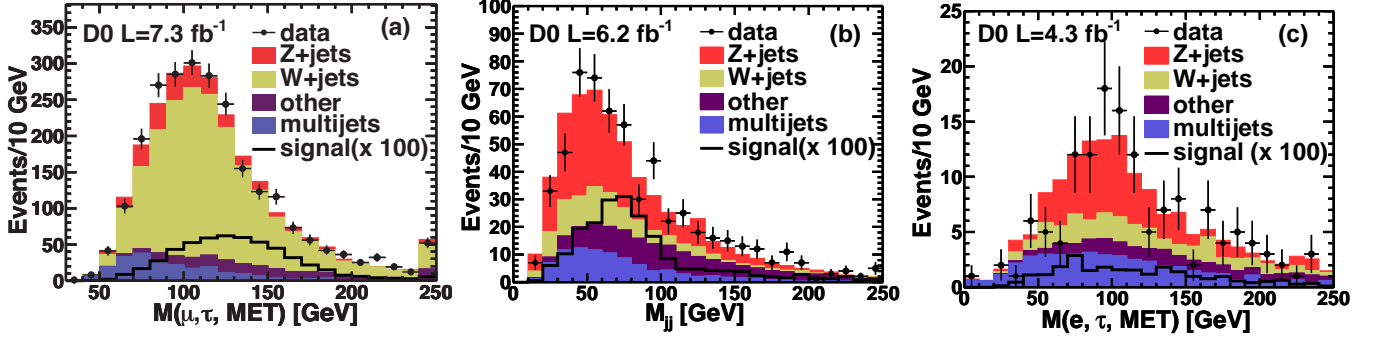


FIG. 2: (color online) Comparison of data, expected backgrounds, and total signal with the indicated scaling factors for (a) invariant mass of the μ, τ, \cancel{E}_T system for the $\mu\tau 0$ analysis (signal shown for $m_H = 165$ GeV); (b) dijet invariant mass for the $\mu\tau 2$ analysis (signal shown for $m_H = 150$ GeV); and (c) invariant mass of the $\tau\tau$ system for the $e\tau 2$ analysis (signal shown for $m_H = 150$ GeV), where the \cancel{E}_T contribution is apportioned to the e and τ as discussed in the text. The “MET” in the labels refers to \cancel{E}_T . The $t\bar{t}$, single top and diboson backgrounds are shown together as “other”.

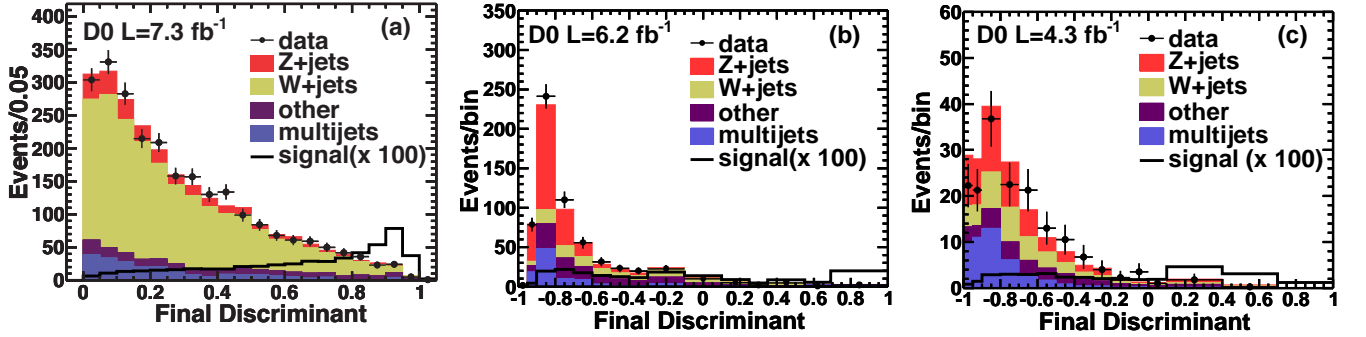


FIG. 3: (color online) (a) NN_H distribution for the $\mu\tau 0$ analysis at $m_H = 165$ GeV; (b) BDT distribution for the $\mu\tau 2$ analysis at $m_H = 150$ GeV; and (c) BDT distribution for the $e\tau 2$ analysis at $m_H = 150$ GeV. The $t\bar{t}$, single top and diboson backgrounds are shown together as “other”.

GeV steps, averaged over neighboring mass bins as described above.

The impact of systematic uncertainties on the limits is minimized by maximizing a likelihood function [30] in which these uncertainties are constrained to Gaussian priors. The value of the Higgs boson cross section is adjusted in each limit calculation until the value of CL_s reaches 0.05, corresponding to the 95% C.L., where $CL_s = CL_{s+b}/CL_b$ and CL_{s+b} (CL_b) are the probabilities for the negative LLR value observed in simulated signal+background (background) pseudo-experiments to be less than that observed in our data. The limits obtained are summarized in Table IV.

We combine the information from the three channels by recomputing the LLR and limits for the three analyses together, now also including the limits from the previous independent $\mu\tau 2$ analysis using 1 fb^{-1} [6]. In this calculation, the systematic uncertainties across the different analyses are appropriately correlated (e.g. the Z + jets normalization for all channels is the same). The fully combined LLR distributions and the 95% C.L. limits as

a function of m_H are shown in Figs. 4 and 5. The combined limits are also shown in Table IV.

In summary we have searched for the SM Higgs boson in final states involving an electron or muon and a hadronically decaying tau. We set 95% C.L. limits on the Higgs boson production cross section which are 21.8 and 6.8 times those expected in the SM for Higgs boson masses of 115 and 165 GeV.

We thank the staffs at Fermilab and collaborating institutions, and acknowledge support from the DOE and NSF (USA); CEA and CNRS/IN2P3 (France); MON, Rosatom and RFBR (Russia); CNPq, FAPERJ, FAPESP and FUNDUNESP (Brazil); DAE and DST (India); Colciencias (Colombia); CONACyT (Mexico); NRF (Korea); FOM (The Netherlands); STFC and the Royal Society (United Kingdom); MSMT and GACR (Czech Republic); BMBF and DFG (Germany); SFI (Ireland); The Swedish Research Council (Sweden); and CAS and CNSF (China).

TABLE III: The range of systematic uncertainties (in percent) for categories of their source. Each category generally summarizes several individual sources separated by analysis channel, tau type, and/or physical process. Those with “N” affect only the normalization of the final variable distribution. Those indicated as “S” also affect the shape of the final variable distribution.

Source	Type	Uncertainty
Luminosity	N	6.1
Muon trigger	N	5 – 9
Electron trigger	N	2
Muon reconstruction	N	2 – 3
Electron reconstruction	N	4
Tau reconstruction	N	4 – 14
Jet reconstruction	S	2 – 10
Jet modeling	S	0 – 7
MC simulated backgrounds	N	5 – 12
MJ background	S	10 – 50
Signal cross sections	N	5 – 40

TABLE IV: The ratio of expected and observed 95% C.L. limits on the Higgs boson cross section to the SM values for each analysis channel and the combination of all channels including that of [6].

m_H	$\mu\tau 0$		$\mu\tau 2$		$e\tau 2$		Combined	
	exp	obs	exp	obs	exp	obs	exp	obs
105	–	–	17.7	18.5	33.3	58.9	12.6	17.1
110	–	–	19.3	20.8	34.3	55.7	12.9	17.7
115	84.2	106.4	20.3	26.3	37.5	55.1	14.3	21.8
120	42.9	31.1	19.2	23.3	40.5	59.4	13.7	15.6
125	34.2	37.5	17.3	19.5	42.3	64.9	12.8	15.7
130	25.2	32.4	15.9	20.6	44.2	72.5	11.5	17.9
135	20.3	20.3	17.5	15.2	47.2	82.5	11.3	11.8
140	16.7	20.0	18.7	13.2	44.7	68.1	11.1	10.1
145	13.8	13.3	18.3	12.9	43.5	54.2	11.3	9.8
150	11.9	12.8	17.9	13.6	45.4	54.1	10.8	9.5
155	9.8	12.9	18.2	13.2	42.3	57.5	9.2	9.0
160	8.2	7.6	19.1	11.1	33.9	74.9	8.4	7.6
165	8.1	7.8	21.7	11.2	32.8	69.8	7.7	6.8
170	8.5	9.4	21.3	12.7	35.2	64.5	8.5	7.4
175	9.5	8.6	22.7	11.4	40.7	73.7	9.6	8.0
180	12.2	13.5	22.1	14.6	45.5	84.6	11.4	11.0
185	13.5	12.1	25.7	19.8	53.7	90.8	12.2	9.7
190	16.5	17.2	29.5	19.1	58.8	101.8	14.6	12.3
195	18.5	18.7	30.1	20.9	67.3	110.4	16.1	15.3
200	19.2	31.5	28.9	26.9	69.3	114.4	19.8	29.9

-
- [1] R. Barate *et al.* (LEP Working Group for Higgs boson searches), Phys. Lett. B **565**, 61 (2003).
[2] T. Aaltonen *et al.* (CDF and D0 Collaborations), Phys. Rev. Lett. **104**, 061802 (2010).
[3] The ATLAS Collaboration, [arXiv:hep-ex/1202.1408](#) (2012); the CMS Collaboration, [arXiv:hep-ex/1202.1488](#) (2012).
[4] M. Baak *et al.* (GFitter collaboration), [arXiv:hep-ph/1107.0975](#) (2011), (submitted to Eur. Phys. J. C).
[5] With new measurements of the W boson mass, T. Aaltonen *et al.* (CDF Collaboration), [arXiv:hep-ex/1203.0275](#) and V.M. Abazov *et al.* (D0 Collaboration), [arXiv:hep-ex/1203.0293](#), the con-

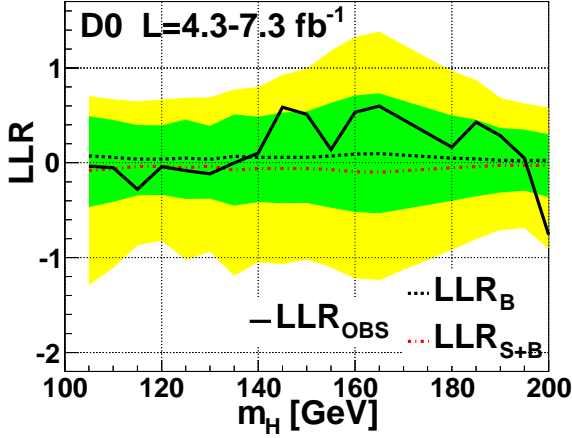


FIG. 4: (color online) The LLR distribution as a function of m_H showing the expected LLR distributions for the background only and signal+background hypotheses, and the observed LLR, for the combination of all channels. The green (yellow) bands show the ± 1 s.d. (± 2 s.d.) bands around the expected background only LLR values.

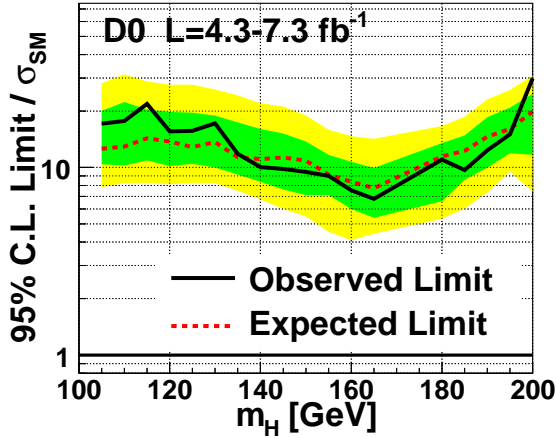


FIG. 5: (color online) The ratio of observed and expected Higgs boson cross section limits to those expected in the SM, for the combination of all channels. The green (yellow) bands show the ± 1 s.d. (± 2 s.d.) bands around the expected ratios.

straints on m_H from precision measurements are reduced by about 5%.

- [6] V.M. Abazov *et al.* (D0 Collaboration), Phys. Rev. Lett. **102**, 251801 (2009).
- [7] S. Abachi *et al.* (D0 Collaboration), Nucl. Instrum. Meth-

- ods Phys. Res. A **338**, 185 (1994); V.M. Abazov *et al.* (D0 Collaboration), Nucl. Instrum. Methods Phys. Res. A **565**, 463 (2006); V.M. Abazov *et al.*, Nucl. Instrum. Methods Phys. Res. A **584**, 75 (2008); and V.M. Abazov *et al.*, Nucl. Instrum. Methods Phys. Res. A **622**, 298 (2010).
- [8] J. Pumplin *et al.*, J. High Energy Phys. **07**, 012 (2002).
- [9] M.L. Mangano *et al.*, J. High Energy Phys. **07**, 001 (2003).
- [10] T. Sjöstrand, S. Mrenna and P. Skands, J. High Energy Phys. **05**, 026 (2006).
- [11] V.M. Abazov *et al.* (D0 Collaboration), Phys. Rev. Lett. **100**, 102002 (2008).
- [12] K. Melnikov and F. Petriello, Phys. Rev. D **74**, 114017 (2006).
- [13] R. Hamburg, W.L. van Neerven, and W.B. Kilgore, Nucl. Phys. **B359**, 343 (1991); **B644**, 403 (2002).
- [14] A.D. Martin, R.G. Roberts, W.J. Stirling, and W.B. Kilgore, Phys. Lett. B **604**, 61 (2004).
- [15] E. Boos *et al.*, Phys. Atom. Nucl. **69**, 1317 (2006); E. Boos *et al.* (CompHEP Collaboration), Nucl. Instrum. Methods Phys. Res. A **534**, 250 (2004).
- [16] N. Kidonakis, Phys. Rev. D **74**, 114012 (2006); S. Moch and P. Uwer, Phys. Rev. D **78**, 34003 (2008).
- [17] J. Baglio and A. Djouadi, J. High Energy Phys. **10**, 064 (2010).
- [18] A. Djouadi, J. Kalinowski, and M. Spira, Comp. Phys. Commun. **108**, 56 (1998).
- [19] S. Jadach *et al.*, Comp. Phys. Commun. **76**, 361 (1993).
- [20] R. Brun and F. Carminati, CERN Program Library Long Witeup W5013, 1993 (unpublished).
- [21] The primary vertex is that found to be the most likely collision point, among possibly several collisions within a specific beam crossing, from which our selected objects emanate. The algorithm for defining it can be found in V. M. Abazov *et al.* (D0 Collaboration), Nucl. Instrum. Methods Phys. Res. A **620**, 490 (2010).
- [22] V.M. Abazov *et al.* (D0 Collaboration), Phys. Lett. B **670**, 292 (2009).
- [23] G. Blazey *et al.* in *Proceedings of the Workshop: QCD and Weak Boson Physics in Run II*, edited by U. Baur, R.K. Ellis and D. Zeppenfeld, Fermilab-Pub-00/297 (2000).
- [24] D. Rainwater, D. Zeppenfeld, K. Hagiwara, Phys. Rev. D **59**, 014037 (1999).
- [25] V.M. Abazov *et al.* (D0 Collaboration), Phys. Rev. Lett. **101**, 071804 (2008).
- [26] A. Schwartzman, FERMILAB-THESIS-2004-21 (2004).
- [27] R. Madar, FERMILAB-THESIS-2011-39 (2011).
- [28] A. Höcker *et al.*, [arXiv:physics/0703039v5](https://arxiv.org/abs/physics/0703039v5) (2007).
- [29] A. Read, J. Phys. G: Nucl. Part. Phys. **28**, 2693 (2002); T. Junk, Nucl. Instrum. Methods Phys. Res. A **434**, 435 (1999).
- [30] W. Fisher, FERMILAB-TM-2386-E (2007).